

Article

Fire Affects Tree Growth, Water Use Efficiency and Carbon Sequestration Ecosystem Service of *Pinus nigra* Arnold: A Combined Satellite and Ground-Based Study in Central Italy

Francesco Niccoli , Simona Altieri * , Jerzy Piotr Kabala  and Giovanna Battipaglia 

Department of Environmental, Biological and Pharmaceutical Sciences and Technologies, University of Campania "L. Vanvitelli", Via Vivaldi 43, 81100 Caserta, Italy; francesco.niccoli@unicampania.it (F.N.); jertzypiotr.kabala@unicampania.it (J.P.K.); giovanna.battipaglia@unicampania.it (G.B.)

* Correspondence: simona.altieri@unicampania.it

Abstract: The Mediterranean basin is an area particularly exposed to fire risk due to its climate and fire-prone vegetation. In recent decades, the frequency and intensity of wildfires increased, leading to negative effects on forests, such as a decrease in tree growth or an increase in tree mortality, producing a relevant loss of carbon sequestration ecosystem service. This study of the impacts of fires on forests is fundamental for planning adequate forest management strategies aimed at recovering and restoring the affected areas. In this framework, our research delves into the effects of a forest fire that, in 2017, affected a forest of black pine (*Pinus nigra* Arnold) in Central Italy. Combining satellite and terrestrial analyses, this study evaluated the impact of the fire on tree growth, water use efficiency and carbon sequestration capacity. Our findings highlight the importance of using remote sensing for the accurate identification of fire-affected areas and precise planning of ground-based activities. However, the integration of satellite data with forest surveys and sampling has proven crucial for a detailed understanding of fire's effects on trees. Dendrochronology and stable isotopes have revealed the post-fire growth decline and altered water usage of defoliated trees. Furthermore, the quantification of CO₂ sequestration highlighted a significant reduction in carbon uptake by damaged trees, with severe implications for this ecosystem service.

Keywords: intrinsic water use efficiency; satellite analysis; tree-ring; stable isotope; forest-fire



Citation: Niccoli, F.; Altieri, S.; Kabala, J.P.; Battipaglia, G. Fire Affects Tree Growth, Water Use Efficiency and Carbon Sequestration Ecosystem Service of *Pinus nigra* Arnold: A Combined Satellite and Ground-Based Study in Central Italy. *Forests* **2023**, *14*, 2033. <https://doi.org/10.3390/f14102033>

Academic Editor: Sara Marañón Jiménez

Received: 5 September 2023

Revised: 3 October 2023

Accepted: 10 October 2023

Published: 11 October 2023



Copyright: © 2023 by the authors. Licensee MDPI, Basel, Switzerland. This article is an open access article distributed under the terms and conditions of the Creative Commons Attribution (CC BY) license (<https://creativecommons.org/licenses/by/4.0/>).

1. Introduction

The Mediterranean basin is considered to be a wildfire hotspot due to its characteristic climatic conditions and fire-prone forest vegetation [1]. In recent years, due to climate change, the frequency, intensity, and spatial extent of fires in this area have increased, with serious ecological, economic, and social consequences [2,3]. Although fires play a crucial ecological role for Mediterranean vegetation [4], severe damage to plant tissues can have negative effects on the eco-physiological functioning of trees, resulting in decreased growth, impaired photosynthesis rates, and tree mortality [5,6]. The degree of damage to trees is directly correlated with the severity of the forest fire [7]. High-severity fires could lead to significant trunk damage and complete destruction of a tree's canopy, resulting in immediate tree death [8]. Conversely, fires of low or moderate severity may not kill the trees in the short term, but they can affect tree's physiology and exacerbate existing climate stresses, increasing plants' vulnerability in the middle and long term [9–11].

The study of forest fires is of fundamental importance for the preservation of forest ecosystem services. In fact, when considered at a population level, the impacts of forest fires significantly alter the ecological functions provided by forests, such as regulation of the hydrological cycle, provision of food and timber products, soil stability, and biodiversity conservation [12]. Moreover, the physiological dysfunctions or even deaths of trees caused by fires greatly reduce forests' capability to sequester CO₂ from the atmosphere and,

consequently, to counteract climate change [13]. Therefore, it is essential to accurately identify and promptly map areas affected by fire, as well as to have a comprehensive understanding of the eco-physiological impacts of fires on key trees species. This knowledge is crucial for implementing effective post-fire management practices in fire-affected areas and developing suitable landscape management strategies for future fire regimes [14].

To evaluate the impact of a fire on forests, surveys and land-based measurements are essential. In this context, dendrochronological analyses are widely used to study how tree species respond to various fire regimes [7,15–19]. Tree rings provide valuable growth information, enabling the reconstruction of carbon allocation capacity over time and determining if it was affected by stress events such as fire [20,21]. Dendrochronology studies are often combined with stable carbon isotope analyses in tree rings to assess the intrinsic water use efficiency (WUEi) of forests [22,23]. The examination of tree WUEi, which is the ratio between net photosynthetic velocity and stomatal conductance, enhances our understanding of the eco-physiological effects of fires [24].

In recent years, the advancement of new technologies has facilitated the integration of land-based studies with remote sensing data. The use of satellite data in the ecological field has greatly contributed to the development of studies of forest fires, allowing a precise assessment of their extent, intensity, and severity regarding forest resources [25]. From the comparison of the pre- and post-fire satellite images, it is possible not only to quantify the immediate impacts of fire on forests but also to evaluate the vegetation recovery in the following years [26]. One of the most used satellite indices is the Normalized Burn Ratio (NBR), which allows us to identify burned area and measure burn severity [27,28]. Similarly, the Normalized Difference Vegetation Index (NDVI), derived from optical remote sensing imagery, is often used to quantify vegetation greenness and assess variations in plant density and health [29]. Therefore, this index can be highly useful for monitoring post-fire vegetation dynamics: the usage of data obtained from satellite image allows us to organize precise land-based forest survey campaigns to study fires [30] and plan immediate forest management interventions [31].

Our research aimed to understand the impacts of a forest fire that affected a stand of *Pinus nigra* Arnold (black pine) on Monte Cairo in Central Italy in July 2017, combining satellite information and land-based forest surveys. Our goal was to use the satellite images to discriminate, within a large forest area affected by the fire, the stands in which trees had experienced significant defoliation due to fire compared to stands where trees were not severely affected. Based on this mapping, we conducted a structural survey in the field and dendrochronological sampling to evaluate the impacts of the fire on growth and water use efficiency of the trees, as well as on the ability of the stands to sequester CO₂ from the atmosphere in the post-fire years. We expect the identification of the more damaged areas via the NBR to be confirmed via ground surveys, with a higher degree of defoliation and tree mortality. Furthermore, we hypothesize that the fire has negatively affected the efficiency of water use and the carbon allocation for the growth of defoliated trees, thus resulting in a serious negative impact on forest ecosystem services.

2. Materials and Methods

2.1. Study Area

The study area is located on the Monte Cairo (1669 m asl) massif of the Lazio region in Central Italy (Figure 1A). This area is characterized by a typical Mediterranean climate, with mild and wet winters and hot and dry summers: the average temperature and precipitation in the last 50 years were 13.1 °C and 1267 mm/year, respectively (the thermo-pluviometric diagram of the study area is reported in Supplementary Material Figure S1). The forest vegetation of Monte Cairo is mainly composed, at the lowest elevation, of sporadic stands of *Castanea sativa* and deciduous oak forests of *Quercus ilex*, *Quercus pubescens*, and *Quercus cerris*. At higher elevations, on the southwestern slopes, stands of *Pinus nigra* occur, while in the highest and less accessible areas, *Fagus sylvatica* forests are present (Figure 1B).

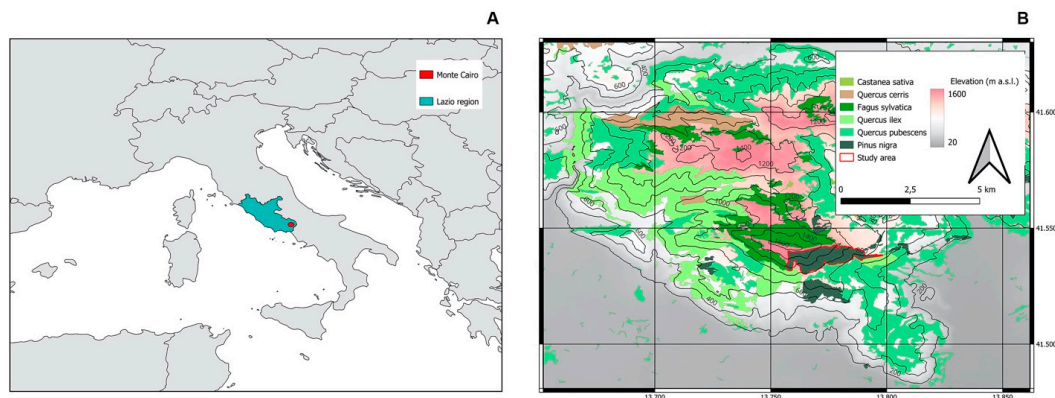


Figure 1. (A) Location of Monte Cairo (red dot) within the Lazio region (in blue), in the center of the Mediterranean basin. (B) Forest vegetation map of Monte Cairo: the *Pinus nigra* pine forest under study is delimited in red.

Our research focused on the *Pinus nigra* forest planted around 1970 and covering an approximate area of 223 ha along the slope of Monte Cairo (41.573° N, 13.773° E). This forest is located at altitudes ranging from 700 to 1550 m above sea level in the municipality of Terelle (Frosinone), characterized by even-aged trees (with an average age of 50 years) that are uniformly distributed (the pre-fire tree density was around 400 trees per hectare), as well as by an undergrowth with sparse herbaceous and shrubby plants. At the end of July 2017, this population has been hit by a severe wildfire, classifiable as a crown fire, which affected several hectares of the *Pinus nigra* forest, causing serious damage to the tree canopy, scorching the trunk and showing blackening on the bark.

2.2. Mapping of the Fire Damage from Satellite Imagery

In order to identify the areas burned in 2017 and provide a measure of burn severity, the Normalized Burn Ratio (NBR) was used. Two images from the Landsat 8 database were chosen for this purpose, with one representing the pre-fire condition and the other one representing the post-fire condition. These images were downloaded from the Earth Explorer portal (<https://earthexplorer.usgs.gov/>, accessed on 1 June 2023) as Level 2 surface reflectance data [32]. For post-fire, the image recorded on 19 October 2017 was chosen. For pre-fire, the image recorded on 1 November 2016 was used to minimize the effect of vegetation phenology on the assessment procedure.

For each selected satellite image, the NBR was computed following Equation (1), and the difference between the pre-fire and post-fire (hereafter dNBR) was calculated, following Equation (2) [33].

$$\text{NBR} = (\text{NIR} - \text{SWIR}) / (\text{NIR} + \text{SWIR}) \quad (1)$$

$$\text{dNBR} = (\text{NBR}_{\text{pre}} - \text{NBR}_{\text{post}}) \quad (2)$$

where NIR is the near infrared, which corresponds to the Band 5 of the Landsat 8 OLI sensor, recorded in the 851–879 nm wavelength; while SWIR is the short-wave infrared, which corresponds to the Band 7 of the Landsat 8 OLI sensor, recorded in the 2107–2294 nm wavelength.

The dNBR was used to discriminate between defoliated stands (DS) and non-defoliated stands (NS) within the *Pinus nigra* forest after the 2017 fire according to the table proposed by USGS [34]. The procedure was performed using QGIS software, version 3.22.

To assess the dynamics of post-fire forest vegetation over the years, we computed the Normalized Difference Vegetation Index (NDVI) values for the DS and NS areas. The satellite imagery used were obtained from LANDSAT 8 via Google Earth Engine (accessed on 1 June 2023). Data from 2013 to 2022 were utilized, selecting only images not affected by cloudiness over the study area. The computation of NDVI, as a measure of canopy greenness, was performed for the DS and NS areas. Subsequently, the mean annual NDVI

values, excluding outliers, along with their corresponding relative standard deviation, were graphically represented for each area. The equation used for NDVI calculation is as follows:

$$\text{NDVI} = (\text{NIR} - \text{R}) / (\text{NIR} + \text{R}) \quad (3)$$

where NIR represents the near-infrared reflectance (LANDSAT 8 band 5), and R corresponds to the visible red reflectance (LANDSAT 8 band 4).

2.3. Field Surveys and Sampling Campaign

After the elaboration of the fire damage map, land-based surveys and sampling operations were carried out. For the two identified areas (DS and NS), three random experimental plots, each with a diameter of 20 m (surface of 314 m²), were selected. In order to ensure consistent comparison, the experimental plots were positioned at the same altitude of 1200 m above sea level. In each plot, the total number of trees was counted, and for each tree, the diameter at breast height (DBH) and the height were measured. Dead trees, when present, were counted and measured. Furthermore, the heights of trunk scorching were measured, as well as the potential tree crown defoliation, through visual estimation [7]. Finally, dendrochronological samples were collected in each experimental plot using an incremental borer (Haglöfs, Långsele, Sweden). For both DS and NS, a total of 10 dominant trees were chosen, from which two wood-cores were taken in the southern and western directions, following standard procedures [35].

2.4. Dendrochronological Measurement and Processing Data

The collected wood cores were mounted on dedicated supports and underwent a sanding process to facilitate the identification of tree rings. The measurement of ring widths was carried out using the LINTAB system, a stereomicroscope connected to a computer equipped with TSAP-Win software, enabling the analysis and processing of dendrochronological curves that represent the growth of each individual tree. After measuring each sample, a statistical comparison of the curves was conducted, utilizing cross-dating through the Gleichaufigkeit index (GLK), which assesses the correlation between different series [36]. Afterwards, the Basal Area Increment (BAI) was calculated from the raw chronologies. BAI is a sensitive and biologically meaningful indicator of tree growth, widely utilized for evaluating the impacts of stressful events on forests and trees [23,37]. Indeed, BAI series helped to minimize the influence of tree size and age on annual growth patterns while preserving the high- and low-frequency signals embedded within the tree-ring series [38]. BAI was computed using the following equation:

$$\text{BAI}_t = \pi r_t^2 - \pi r_{t-1}^2 \quad (4)$$

where BAI at year t is equal to the annual ring area (expressed as cm²), r represents the radius of the stem at the end of the annual increment, and r_{t-1} represents the stem radius at the beginning of the growing season.

The BAI of the trees in DS was compared to that in NS in the five years before the fire event to test whether both groups previously had the same growth rate. It was then compared to the five years after the fire to check if any differences appeared after the fire event. The t -test was used to compare the two groups. The dendrochronological data analyses were performed in R using the dplR library [39,40].

Finally, to evaluate the influence of the climatic conditions of Monte Cairo on the *Pinus nigra* stands, the correlation was tested between the BAI data of DS and NS in the pre-fire period (1970–2017) and meteorological data (maximum, minimum, and mean temperature, and precipitation) obtained from the ERA5-Land database with a spatial resolution of 11 km [41]; the ERA5 data for the study area were extracted via Google Earth Engine (accessed 1 June 2023) [42]. Data of post-fire years (2018–2022) were excluded to prevent the fire event from affecting the correlation results. The correlation test was performed

using the *dcc* and *seascorr* functions of the *treeclim* package in RStudio environment [43] to test the correlations both monthly and seasonally [44].

2.5. Intrinsic Water Use Efficiency Analyses

For the two selected areas, DS and NS, six wood cores were selected based on their strong cross-dating ($GLK > 0.70$) with the corresponding reference chronology in order to perform the WUEi analysis. The annual rings of the last 10 years (2013–2022) were carefully separated using a blade cutter and grounded using a pulverizing mill (ZM 1000, Retsch, Haan, Germany), with a mesh size of 0.5 mm used to ensure homogeneity. Then, samples were precisely weighed in tin capsules for the $\delta^{13}C$ measurements. The carbon isotope composition was determined at the Iona Laboratory (University of Campania, Caserta, Italy) by means of an isotope ratio mass spectrometer (Delta V Advantage, Thermo Scientific, Waltham, MA, USA) connected in continuous flow to an elemental analyzer (EA 1112 series, Thermo Scientific). The $\delta^{13}C$ measurements were calibrated using certified international standards, and the standard deviation of the repeated analysis of an internal standard was less than 0.1‰ for $\delta^{13}C$. Carbon isotopic ratios are expressed using the delta notation:

$$\delta^{13}C_{\text{plant}} = \delta^{13}C_{\text{atm}} - a - (b - a) \times c_i / c_a \quad (5)$$

where *a* represents the fractionation factor due to CO₂ diffusion through stomata (4.4‰), while *b* represents the fractionation factor due to the Rubisco enzyme during photosynthesis (27‰). *c_a* and *c_i* are atmospheric and leaf intracellular space CO₂ concentrations, and 1.6 is the ratio of the diffusivities of water and CO₂ in the atmosphere.

After measuring the $\delta^{13}C$ values, they were utilized to calculate the WUEi, which represents the ratio between net photosynthesis (*A*) and stomatal conductance (*g_s*) [45]:

$$WUEi = A / g_s = (c_a - c_i) / 1.6 \quad (6)$$

The calculation of carbon isotope discrimination (Δ) was performed based on the difference between the isotopic carbon values of atmospheric CO₂ ($\delta^{13}C_{\text{atm}}$) and plant organic matter ($\delta^{13}C_{\text{plant}}$):

$$\Delta = (\delta^{13}C_{\text{atm}} - \delta^{13}C_{\text{plant}}) / (1 + \delta^{13}C_{\text{plant}}) \quad (7)$$

The $\delta^{13}C_{\text{atm}}$ data could be obtained from online archives (<http://www.esrl.noaa.gov/>, accessed on 1 June 2023), while $\delta^{13}C_{\text{plant}}$ data referred to those measured in tree rings.

By combining Equations (5) and (7), we can obtain the value of *c_i* as follows:

$$c_i = c_a [(\Delta - a) / (b - a)] \quad (8)$$

Finally, replacing the Equation (8) in (6), we obtained the following equation:

$$WUEi = (c_a - c_i) / 1.6 = [c_a - c_a(\Delta - a / b - a)] / 1.6 = c_a [(1 - (\Delta - a / b - a)) / 1.6] \quad (9)$$

Once WUEi data were obtained, the relationships between the growth and water use of trees in DS and NS were evaluated by performing correlation tests with BAI. Furthermore, to assess the post-fire intrinsic water use efficiency responses of trees in DS and NS, we used WUEi data to calculate the resistance, resilience, and recovery indices [46].

The resistance index was calculated as the ratio between the WUEi in the year of the fire (WUEi disturbance) and the average of WUEi in the pre-fire years (WUEi pre-disturbance).

$$WUEi \text{ Resistance index} = WUEi_{\text{disturbance}} / WUEi_{\text{pre-disturbance}} \quad (10)$$

Further, the resilience index was calculated by dividing the average WUEi value in the post-fire years (WUEi post-disturbance) by the WUEi pre-disturbance.

$$WUEi \text{ Resilience index} = WUEi_{\text{post-disturbance}} / WUEi_{\text{pre-disturbance}} \quad (11)$$

Conversely, the recovery index was computed by dividing the values of each post-fire year by the WUEI disturbance.

$$\text{WUEi Recovery index} = \text{WUEi}_{\text{post-disturbance}} / \text{WUEi}_{\text{disturbance}} \quad (12)$$

Finally, Student's *t*-test was used to compare these indices between the two areas. All the statistical analyses were performed using R-studio [47].

2.6. Backdating of Structural Stand Data and Atmospheric CO₂ Sequestration

The tree ring width data were used to infer the past DBH of the examined trees. The DBH for each year was estimated by progressively subtracting the sum of the ring widths from the DBH measured at the end of 2022. The tree height chronology was estimated from the DBH using the Chapman Richards allometric equation [48]. The total above ground biomass (AGB) of trees was then computed using the equations from the Italian Forest inventory, which are implemented in the ForIT R package [49]:

$$\text{AGB} = -33.97 + 1.73 \times 10^{-2} \times \text{DBH}^2 \times \text{TreeHeight} + 4.19 \times \text{DBH} \quad (13)$$

Afterwards, to take into account the belowground biomass, its contribution was calculated considering a belowground-to-aboveground biomass ratio of 0.2 [50]. Furthermore, the biomass was converted to its CO₂ equivalent stored in the trees by multiplying biomass by the Carbon Fraction Value (0.51) and the Carbon-CO₂ conversion factor (3.67), following the guidelines of the IPCC for assessing carbon stored in forest biomass [51]:

$$\text{CO}_2 \text{ stored in the tree} = \text{AGB} \times (1 + 0.2) \times 0.51 \times 3.67 \quad (14)$$

This process allowed the computation of the yearly values of CO₂ fixed as tree biomass as the difference between the biomass at the end of the growing season and the biomass at the end of the previous growing season.

$$\text{CO}_2 \text{ fixed}_t = \text{CO}_2 \text{ stored}_t - \text{CO}_2 \text{ stored}_{t-1} \quad (15)$$

Finally, to assess the economic impacts of the fire on the carbon fixation capacity of Monte Cairo Forest, we calculated the economic value of the CO₂ fixed by the trees in the two areas for the pre-fire and post-fire years. The calculation was performed by multiplying the amount of stored CO₂ by the average spot price of CO₂ in the third quarter of 2022 (80 EUR/tCO₂), as reported in the Quarterly Report on European Electricity Markets released by the European Community [52].

3. Results

3.1. Satellite-Based Computation Analysis

The calculation of the dNBR (difference Normalized Burn Ratio) from the satellite images allowed us to discriminate between the defoliated stands (DS) and the non-defoliated stands (NS) within the extensive *Pinus nigra* forest. The pixels of the map reported in Figure 2A were classified according to their dNBR values: all areas with dNBR values lower than 0.1 were identified as non-defoliated stands (NS, green pixels; total area, 69 ha). On the contrary, all areas with dNBR above this threshold were classified as defoliated stands (DS, orange pixels, total area 154 ha). While the dNBR allowed the assessing of the immediate impact of the fire on the forest, the processing of the Normalized Difference Vegetation Index (NDVI) enabled the analysis of vegetation dynamics over the past 10 years, allowing monitoring of the post-fire trends in the two areas. The time series of NDVI between the two areas (Figure 2B) had a similar trend over the years. In the years prior to the fire, while the NS curve was slightly higher than the DS one, they were not statistically different ($p > 0.05$). However, following the fire event in 2017, a statistically significant divergence in values between NS and DS was found. In fact, the post-fire values of the non-defoliated stands were significantly higher ($p < 0.05$) compared to the defoliated stands.

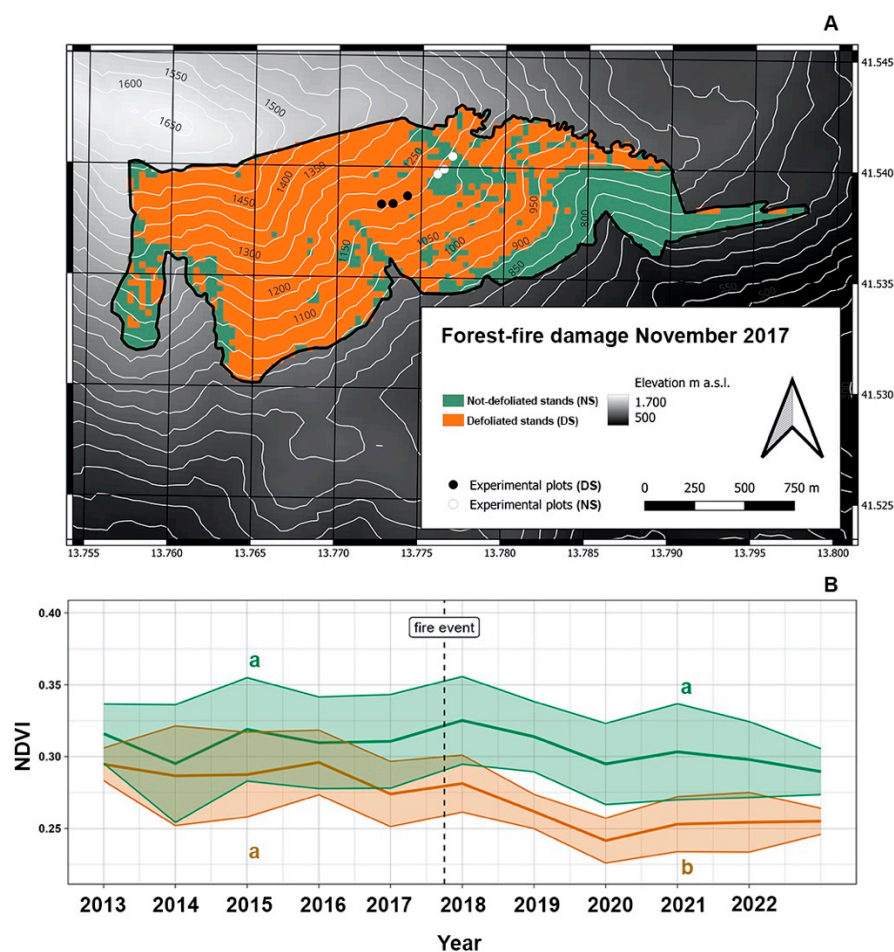


Figure 2. (A) Map of the *Pinus Nigra* Forest of Monte Cairo showing the identification of defoliated stands (DS, orange pixels) and non-defoliated stands (NS, green pixels). The black and white dots indicate the position of the experimental plots in DS and NS, respectively. (B) Mean NDVI time series for DS (in orange) and NS (in green) from 2013 to 2022. The lowercase letters indicate statistical differences between the two areas in the pre- and post-fire periods. The bands indicate the relative standard errors.

3.2. Land-Based Measurements

3.2.1. Forest Survey of the Experimental Plots

Identifying NS and DS enabled us to establish three experimental plots in each category for land-based analysis, all situated at the same altitude and distance from the forest perimeters. Dendrometric measurements conducted in the experimental plots allowed us to collect the structural information of the trees for both areas (Table 1). The two areas showed similar tree heights (in average 22.98 ± 2.48 m for NS and 18.30 ± 4.65 m for DS) and DBH (33.81 ± 5.79 cm for NS and 36.20 ± 8.62 cm for DS). The defoliation observed in the field confirmed the satellite classification: the trees of the NS showed no crown damage, while the trees of the DS had an average crown reduction of around 50%. Trees in both areas showed scorch along the trunk, indicating that the fire also affected the non-defoliated areas, albeit without reaching the tree canopy. Indeed, the mean scorch height was $2.73 + 1.94$ m for NS and $4.65 + 2.59$ m for DS. The post-fire tree density was higher in the NS experimental plots (392 ± 36) compared to the DS experimental plots (276 ± 120) due to the observed tree mortality rate in DS (31%), which caused its reduction. On the contrary, the pre-fire tree density between the two examined areas was more balanced (392 ± 36 for DS, 402 ± 113 for NS). The pre-fire density in DS was calculated by including standing dead trees, which were excluded from the post-fire calculation.

Table 1. Summary of the results of the field survey.

Area	<i>Pinus Nigra</i> Height (m)	<i>Pinus Nigra</i> DBH (cm)	Average Crown Defoliation	Height of Scorch (m)	Tree Density of Pre-Fire Individuals/ha	Tree Density of Post-Fire Individuals/ha	Tree Mortality Rates
Non-defoliated Stands (NS)	22.98 ± 2.4	33.81 ± 5.7	0%	2.73 ± 1.9	392 ± 36	392 ± 36	0%
Defoliated Stands (DS)	18.30 ± 4.6	36.20 ± 8.6	50%	4.65 ± 2.5	402 ± 113	276 ± 120	31%

3.2.2. Dendrochronology Analysis

Dendrochronological analyses have highlighted how the Basal Area Increment (BAI) of the two examined areas was generally highly synchronous over the years (Figure 3A). However, while during the pre-fire period, the growth rates were perfectly overlapping, starting from 2018, a clear divergence in productivity is observed. While statistical tests have revealed that in the five pre-fire years (2013–2017), tree growth between the two areas was comparable ($p > 0.05$), in the five post-fire years (2018–2022), the growth rate was significantly higher ($p < 0.05$) in NS trees (Figure 3B).

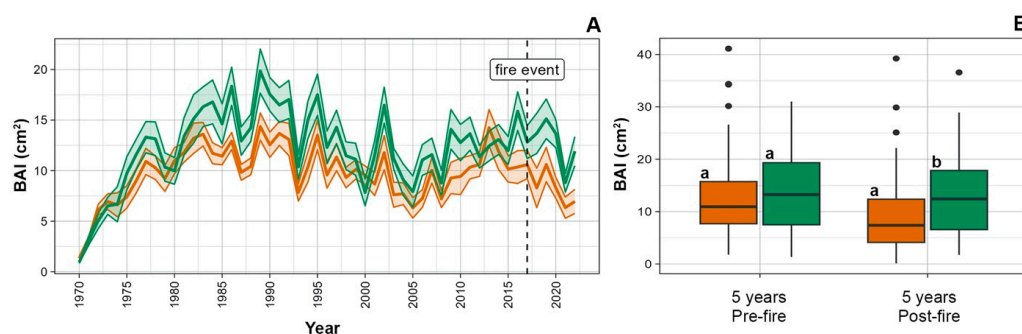


Figure 3. (A) Mean BAI trend recorded in the trees of NS (in green) and DS (in orange). The bands indicate the relative standard error. (B) Comparison between the BAI recorded in the five years pre-fire (2013–2017) and the five years post-fire (2018–2022) of NS (in green) and DS (in orange). The lowercase letters indicate statistical differences between the two areas in the pre- and post-fire periods.

The correlation analyses between the pre-fire BAI (1970–2017) of DS and NS with their respective meteorological data revealed the positive influence of spring temperatures on growth (Figure 4A–C). The temperatures of March (maximum, minimum, and mean for DS; maximum and mean for NS) of the current year showed positive correlations with tree growth in both stands.

Furthermore, we identified negative correlations with the June temperatures for the current year (maximum and mean for DS; maximum and minimum for NS).

Regarding precipitation, no correlations were found for DS, while a negative correlation between growth and precipitation in December of the previous year was evident in NS (Figure 4D). Finally, the seasonal correlation analysis yielded only a negative significant correlation with precipitation of the coldest months (complete results are reported in Supplementary Materials Figure S2).

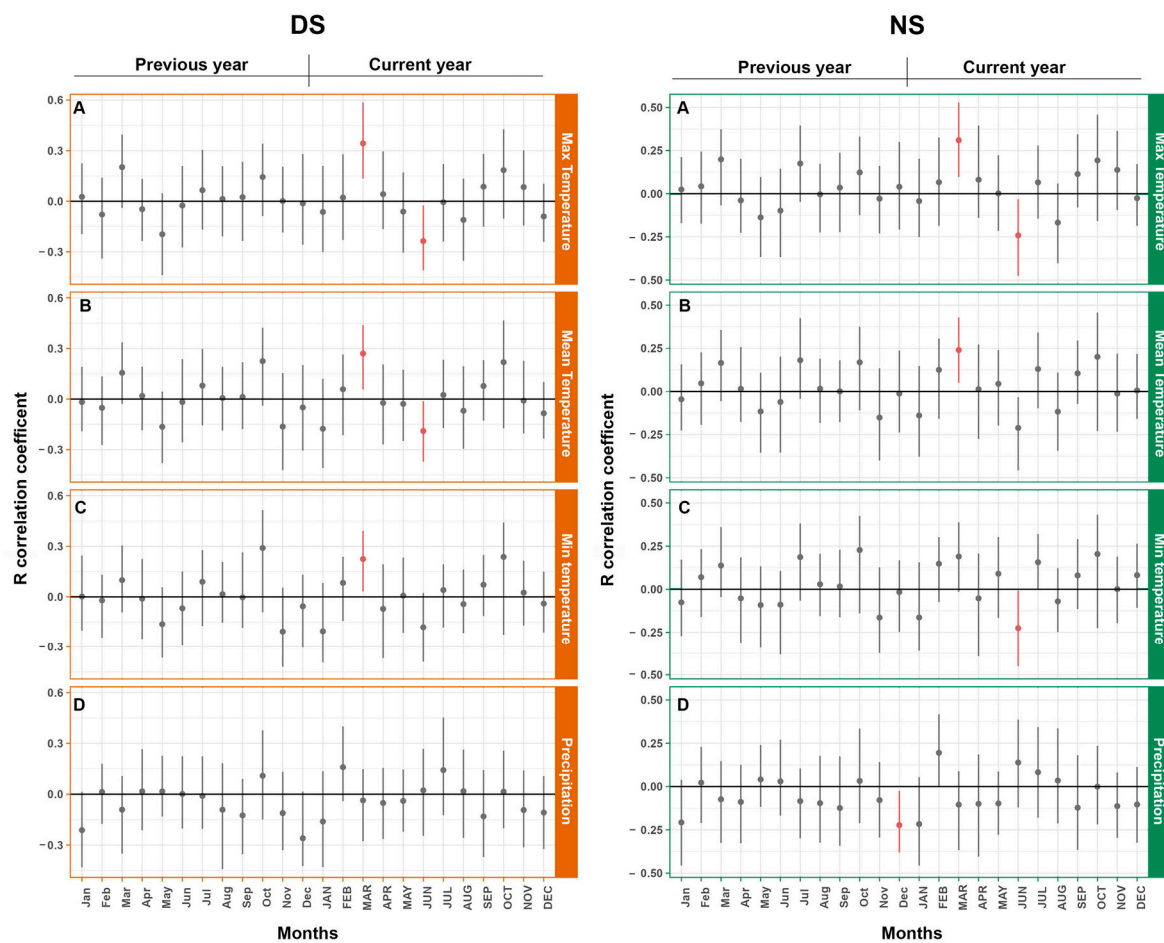


Figure 4. Correlation tests between the pre-fire BAI data (1970–2017) of DS (in orange) and NS (in green) with the relative (A) maximum, (B) minimum, (C) mean temperatures, and (D) precipitation obtained from ERA5 database. Red bars indicate significant correlations ($p < 0.05$), while gray bars indicate no correlations ($p > 0.05$).

3.2.3. Growth–WUE_i Relationship and Responses in Short-to-Medium Term

The relationship between WUE_i and BAI (Figure 5A), tested over the last 10 years (2013–2022), highlighted a significant positive correlation ($p < 0.05$) for the trees in NS: an increase in growth was coupled with an enhancement in water use efficiency. Conversely, in trees of DS, no correlation was observed ($p > 0.05$). The indices of resistance, resilience, and recovery (Figure 5B) calculated using the WUE_i data showed that while the resistance index revealed a similar response to the fire event in both NS and DS ($p > 0.05$), trees in NS showed a better response in terms of resilience and recovery in the years following the fire ($p < 0.05$).

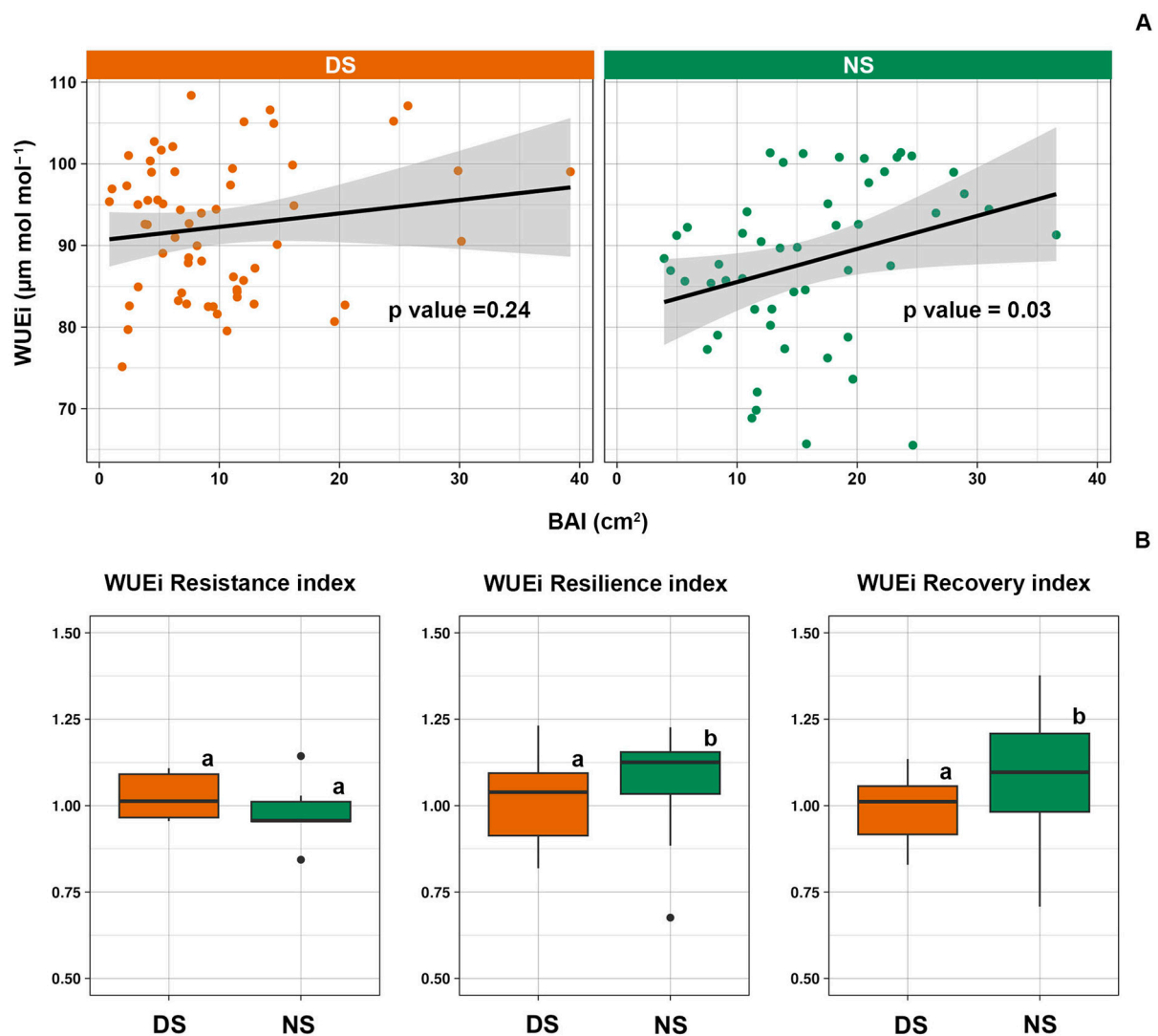


Figure 5. (A) Correlation tests between WUEi and BAI values; (B) resistance, resilience, and recovery indices calculated for trees in DS (in orange) and NS (in green). Reference period: 2013–2022. The lowercase letters indicate statistical differences between the two areas.

3.2.4. CO₂ Sequestration and Ecosystem Service Costs

The estimation of CO₂ sequestered by the trees in the NS and DS (Figure 6A) is in line with tree growth data. Although, over the years, the amount of CO₂ absorbed by the two stands was not always comparable (as evident from 1980 to 1992), during the pre-fire years (2013–2017), the carbon fixation capacity of the trees was statistically the same ($p > 0.05$). Conversely, in the post-fire years (from 2018 to 2022), a clear divergence was evident ($p < 0.05$). Therefore, the economic value of the CO₂ fixed in the five years before the fire was comparable between the two examined areas (ranging from 650 to 1150 EUR/ha). However, starting in 2018 and for all post-fire years, the lower carbon fixation capacity of trees in the DS resulted in a significant decrease in the CO₂ fixed economic value (the values were always around/below 500 EUR/ha, Figure 6B). On the contrary, the trees in the NS had a stable carbon assimilation capacity in these years, retaining a higher service value (ranging from 500 to 1100 EUR/ha).

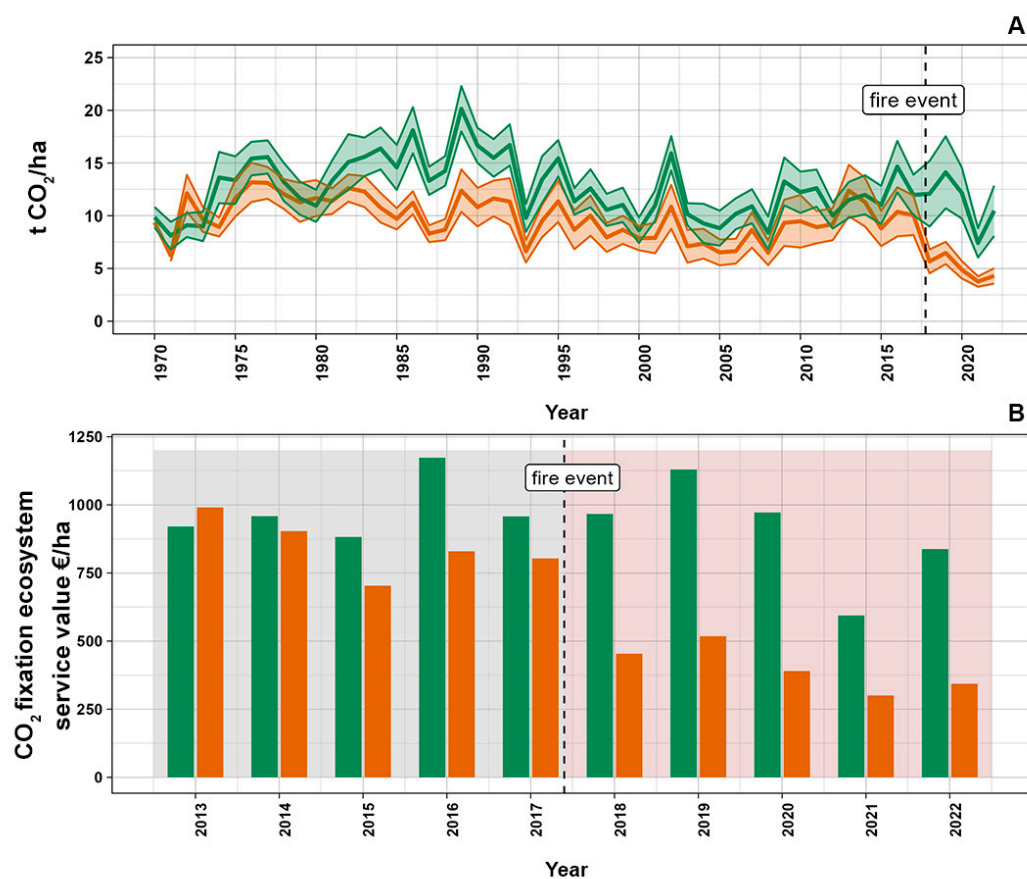


Figure 6. (A) Mean trend of the tons of CO₂ per hectare fixed by the trees in NS (in green) and DS (in orange). The bands indicate the standard error. (B) Economic value, expressed in Euros, of the CO₂ per hectare fixed in the five years pre- and post-fire by the trees in NS (green bars) and DS (orange bars).

4. Discussion

The combination of satellite- and ground-based analyses presented in this study has provided valuable information regarding the understanding of the eco-physiological, ecological, and economic consequences of wildfires on forest ecosystems. Firstly, the use of dNBR (difference Normalized Burn Ratio) based on satellite imagery has been confirmed to be an effective tool for identifying and distinguishing forest areas affected by fire from those remaining relatively intact. The analysis of pre- and post-fire satellite images allowed precise discrimination between defoliated stands (DS) and non-defoliated stands (NS) within a large forest of *Pinus nigra*. This provided a spatially detailed view of the extent of areas affected by the 2017 fire on Monte Cairo and facilitated the strategic planning of a targeted forest survey and ground-based sampling campaign.

The forest surveys on the ground confirmed the correct identification of the two areas: the field measurements highlighted how the discrimination between the two types of areas reflected the crown damage, as well as the reduction in tree density determined based on post-fire mortality rates. While trees in NS did not show defoliation and tree mortality, in DS, we observed strong canopy damage (in average 50%), as well as a rather high tree mortality rate (in average 31%), which significantly reduced the tree density in the years following the fire. These findings are in agreement with previous studies that assessed the effectiveness of the dNBR parameter through field surveys, demonstrating robust correlations with variations in crown structure and forest density [53–55].

Moreover, the results reported in our study highlighted the crucial importance of combining remote sensing analyses with land-based forest survey campaigns. In fact, although the areas have been correctly identified, the field surveys showed that fire also

affected the trees in the NS. The scorch found along the trunk of trees confirmed that NS has been affected by a ground fire, which, however, was not able to damage the crown. As confirmed using the NDVI data, this information was not captured via satellite image analyses in the months and years following the fire, as the low fire severity in the NS did not affect tree density or canopy structure. Indeed, while we observed a significant decline in NDVI, starting in 2017 for the DS, NDVI values were constant in the NS between the years pre- and post-fire.

Further insights have been provided via dendrochronological investigations: while in the years preceding the fire, tree productivity was comparable between the two areas, after the fire event, we observed a clear divergence in growth rates. The strong reduction in growth observed in defoliated trees represents a phenomenon widely reported and investigated in the scientific literature [5,7,11,19,56–58]. This decline in productivity has mainly been attributed to a marked reduction in trees' photosynthetic capacity, which triggers a mechanism known as carbon starvation [15,16]. Severe defoliation results in the lower capacity of trees to uptake atmospheric carbon and produce the necessary carbohydrates to meet the physiological and metabolic demands for their growth and maintenance [59–61]. These mechanisms make trees particularly sensitive to climatic stresses, amplifying their susceptibility to events such as heatwaves and prolonged drought periods, affecting their health and growth [62–64].

The correlations between basal area increment and meteorological data highlighted that although the growth of *Pinus nigra* on Mount Cairo was positively influenced by spring temperatures over the years, the trees were often subjected to intense heatwaves during the summer, as indicated by the negative correlations between growth and temperature observed for the month of June in both DS and NS.

The lack of positive correlation between precipitation and growth, on a monthly and seasonal scale, could be due to the low water retention capacity of the soil, as the forest is located on a steep slope [65]. Furthermore, most of the precipitation occurs during the coldest months, and, thus, its effect on growth is dampened [66].

This supports the hypothesis that the combination of reduced photosynthetic capacity and increased sensitivity to climatic stress has led to a reduction in the growth of trees in DS. In contrast, non-defoliated trees that suffered no photosynthetic damage were able to withstand summer heatwaves. Furthermore, the ground fire might have benefited trees in DS by suppressing undergrowth species, thereby reducing competition for resources [7,16,58].

The WUEi data confirm the previously discussed points. Given that WUEi is an index of the amount of carbon fixed by the plant per unit of water lost through transpiration [67], the strong positive correlation observed between the growth and WUEi of trees in the NS suggests the better capacity of these trees to maintain unchanged photosynthetic rates over the years using a limited amount of water [68]. This reflects a typical strategy of healthy isohydric species growing in drought prone areas such as Monte Cairo, which allows them to grow resiliently, despite climatic stresses, by overcoming periods of limited water availability thanks to their dynamic stomatal control [61,69]. The absence of a correlation between growth and WUEi in defoliated trees confirmed their inability to maintain pre-disturbance photosynthetic rates due to severe canopy injuries [64]. The calculation of tree resistance, resilience, and recovery indices, based on WUEi data, has allowed the establishment of a direct link between tree water use efficiency and their capacity to respond to wildfires in the short and medium term. The resistance index, which assesses the immediate impact of the fire, did not reveal significant differences between trees in NS and DS. Being the same species, fire resistance mechanisms are analogous [70], and this could have triggered the same effects of fire on WUEi in the short term. However, the resilience and recovery indices, which indicate the ability of trees to reach their pre-disturbance conditions, are significantly higher in NS compared to DS. This result suggests a negative effect on the trees' capacity to optimize water use in defoliated trees in the years after the fire [71]. This phenomenon could be attributed to a strategy of greater stomatal opening to counteract the carbon deficit due to strong defoliation suffered by

burned trees [15]. Under normal conditions, stomata play a crucial role in regulating the exchange in CO₂ and water between the plant and its surroundings [72,73]. However, the considerable defoliation experienced by these trees can disrupt this usual pattern: the necessity to assimilate carbon via the reduced canopy may have pushed the trees to increase stomata opening in order to prioritize CO₂ uptake, even at the expense of increased water loss through transpiration [74]. Nevertheless, defoliated trees allocated a limited amount of carbon to growth, suggesting that the resources were prioritized for maintaining metabolic functions [75,76]. Although this strategy ensured their survival, it led to a reduction in post-fire growth and water use efficiency [77,78].

The quantification of the CO₂ sequestered by the trees in the DS and NS, in addition to corroborating our previous interpretations, highlights the ecological and economic impacts of the fire. Although, over the years, the amount of carbon sequestered was not always comparable (such as from 1980 to 1992), probably due events beyond the scope of this study, in the five years preceding the fire event, the CO₂ sequestered between the two sites was statistically similar. However, after the fire, there was a marked decline in defoliated trees absorbing atmospheric carbon.

Forests, under normal conditions, act as important carbon sinks through the process of photosynthesis [79,80]. However, due to fire damage, their ability to perform this crucial role has been significantly impaired in DS. In fact, it was observed that their CO₂ uptake decreased dramatically to approximately half of the levels observed in undamaged trees. A reduced capacity for photosynthesis and CO₂ sequestration implies that a greater amount of carbon dioxide will remain in the atmosphere, contributing to the accumulation of greenhouse gases, which are known to contribute to global warming [81]. The forest carbon sequestration capacity can be quantified through an economic value [82,83]. In the specific case, the ecosystem service of carbon sink of DS—which represent a substantial portion of the total extension of *Pinus nigra* forest on Monte Cairo—has been halved. Therefore, the inability of damaged trees to fully recover their physiological and photosynthetic functions over time, as highlighted in this study, could lead to a gradual reduction in or complete loss of the economic value of the carbon sequestration service. This scenario underscores the importance of adopting responsible and targeted forest management practices to promote the recovery of ecosystems impacted by fires and preserve the long-term economic value of carbon sequestration services.

5. Conclusions

Our insights showed how the dNBR parameter for the initial discrimination of areas affected by fire from those remaining relatively intact is a fundamental tool for assessing fire impacts and planning forest sampling and survey campaigns. Similarly, the NDVI index proved highly reliable in monitoring the evolution of a burned forest. However, our study highlights the crucial role of integrating remote sensing with land surveys for a more precise understanding of tree fire impacts over time.

Dendrochronological and stable isotope analyses shed light on the eco-physiological dynamics of trees in the years following the fire, revealing that defoliated trees reduced their growth and modified their water use due to severe canopy injury.

Finally, the quantification of CO₂ sequestration highlighted the fire's ecological impact. Fire-induced damage has substantially reduced the capacity of defoliated trees to sequester carbon from the atmosphere, reducing their contribution to climate change mitigation. The economic implications of declining carbon stocks have underscored the urgency of employing responsible forest management to mitigate the long-term losses of the carbon sequestration service.

In conclusion, the presented results, albeit based on a single case study, represent a clear example of how the integration of satellite- and ground-based analyses can provide a complete view of the consequences of fires on forest ecosystems, allowing us to achieve several goals aimed at the recovery and restoration of fire-affected areas.

Supplementary Materials: The following supporting information can be downloaded at: <https://www.mdpi.com/article/10.3390/f14102033/s1>, Supplementary Materials Figure S1. Pluvio-thermic plot of the study area, based on the climatic data of the last 50 years. The bars represent the average precipitation of each month, while the red line represents the average temperature, there is indicated also the range between minimum and maximum. Supplementary Materials Figure S2. Seasonal correlations of BAI with precipitation and temperature. Windows of length three, six and nine months were tested. On the x axis, the ending month of the group of the window is indicated in the label. Significant correlations are highlighted in red.

Author Contributions: F.N. and J.P.K. conceived the study, F.N., J.P.K. and G.B. designed the experiment; F.N., J.P.K., S.A. and G.B. performed measurements; F.N., J.P.K., S.A. and G.B. cured data analyses and interpretation; F.N. and S.A. wrote most of the manuscript. All authors wrote specific part of the present version. All authors have read and agreed to the published version of the manuscript.

Funding: This research received no external funding.

Data Availability Statement: The data presented in this study are available on request from the corresponding author.

Acknowledgments: The authors wish to thank the students of Dendrometry class (Sara Mouaouia, Gaetano Pedana, Salvatore De Cunto, Paolo D’Errico, Marzio D’Ambra) for field sampling. This research is linked to activities conducted within the MIUR-PRIN 2017 project “The Italian TREETALKER NETWORK: continuous large scale monitoring of tree functional traits and vulnerabilities to climate change” and the MIUR Project (PRIN 2020) “Unravelling interactions between WATER and carbon cycles during drought and their impact on water resources and forest and grassland ecosystems in the Mediterranean climate (WATERSTEM)” (protocol code: 20202WF53Z).

Conflicts of Interest: The authors declare no conflict of interest.

References

- Senf, C.; Pflugmacher, D.; Zhiqiang, Y.; Sebald, J.; Knorn, J.; Neumann, M.; Hostert, P.; Seidl, R. Canopy Mortality Has Doubled in Europe’s Temperate Forests over the Last Three Decades. *Nat. Commun.* **2018**, *9*, 4978. [[CrossRef](#)] [[PubMed](#)]
- IPCC. *Climate Change 2021: The Physical Science Basis*; IPCC: Geneva, Switzerland, 2021; ISBN 9789291691586.
- Pausas, J.G.; Fernández-Muñoz, S. Fire Regime Changes in the Western Mediterranean Basin: From Fuel-Limited to Drought-driven Fire Regime. *Clim. Chang.* **2012**, *110*, 215–226. [[CrossRef](#)]
- Rundel, P.W. Fire as an Ecological Factor. In *Encyclopedia of Plant Physiology, New Series, Volume 12A. Physiological Plant Ecology. I. Responses to the Physical Environment*; Springer: Berlin/Heidelberg, Germany, 1981; pp. 501–538. [[CrossRef](#)]
- Bär, A.; Michaletz, S.T.; Mayr, S. Fire Effects on Tree Physiology. *New Phytol.* **2019**, *223*, 1728–1741. [[CrossRef](#)]
- Partelli-Feltrin, R.; Smith, A.M.; Adams, H.D.; Kolden, C.A.; Johnson, D.M. Short- and Long-Term Effects of Fire on Stem Hydraulics in *Pinus Ponderosa* Saplings. *Plant Cell Environ.* **2021**, *44*, 696–705. [[CrossRef](#)]
- Niccoli, F.; Esposito, A.; Altieri, S.; Battipaglia, G. Fire Severity Influences Ecophysiological Responses of *Pinus Pinaster* Ait. *Front. Plant Sci.* **2019**, *10*, 539. [[CrossRef](#)] [[PubMed](#)]
- Pausas, J.G.; Keeley, J.E. Epicormic Resprouting in Fire-Prone Ecosystems. *Trends Plant Sci.* **2017**, *22*, 1008–1015. [[CrossRef](#)] [[PubMed](#)]
- Niccoli, F.; Pacheco-Solana, A.; De Micco, V.; Battipaglia, G. Fire Affects Wood Formation Dynamics and Ecophysiology of *Pinus Pinaster* Aiton Growing in a Dry Mediterranean Area. *Dendrochronologia* **2023**, *77*, 126044. [[CrossRef](#)]
- Varner, J.M.; Hood, S.M.; Aubrey, D.P.; Yedinak, K.; Hiers, J.K.; Jolly, W.M.; Shearman, T.M.; McDaniel, J.K.; O’Brien, J.J.; Rowell, E.M. Tree Crown Injury from Wildland Fires: Causes, Measurement and Ecological and Physiological Consequences. *New Phytol.* **2021**, *231*, 1676–1685. [[CrossRef](#)]
- Hood, S.M.; Varner, J.M.; van Mantgem, P.; Cansler, C.A. Fire and Tree Death: Understanding and Improving Modeling of Fire-Induced Tree Mortality. *Environ. Res. Lett.* **2018**, *13*, 113004. [[CrossRef](#)]
- Smith, A.M.; Kolden, C.A.; Tinkham, W.T.; Talhelm, A.F.; Marshall, J.D.; Hudak, A.T.; Boschetti, L.; Falkowski, M.J.; Greenberg, J.A.; Anderson, J.W.; et al. Remote Sensing the Vulnerability of Vegetation in Natural Terrestrial Ecosystems. *Remote Sens. Environ.* **2014**, *154*, 322–337. [[CrossRef](#)]
- Stephens, S.L.; Westerling, A.L.; Hurteau, M.D.; Peery, M.Z.; Schultz, C.A.; Thompson, S. Fire and Climate Change: Conserving Seasonally Dry Forests Is Still Possible. *Front. Ecol. Environ.* **2020**, *18*, 354–360. [[CrossRef](#)]
- Bartowitz, K.J.; Walsh, E.S.; Stenzel, J.E.; Kolden, C.A.; Hudiburg, T.W. Forest Carbon Emission Sources Are Not Equal: Putting Fire, Harvest, and Fossil Fuel Emissions in Context. *Front. For. Glob. Chang.* **2022**, *5*, 867112. [[CrossRef](#)]
- Niccoli, F.; Pacheco-Solana, A.; Delzon, S.; Kabala, J.P.; Asgharinia, S.; Castaldi, S.; Valentini, R.; Battipaglia, G. Effects of Wildfire on Growth, Transpiration and Hydraulic Properties of *Pinus Pinaster* Aiton Forest. *Dendrochronologia* **2023**, *79*, 126086. [[CrossRef](#)]

16. Battipaglia, G.; Strumia, S.; Esposito, A.; Giuditta, E.; Sirignano, C.; Altieri, S.; Rutigliano, F.A. The Effects of Prescribed Burning on *Pinus Halepensis* Mill. as Revealed by Dendrochronological and Isotopic Analyses. *For. Ecol. Manag.* **2014**, *334*, 201–208. [[CrossRef](#)]
17. Valor, T.; González-Olabarria, J.R.; Piqué, M. Assessing the Impact of Prescribed Burning on the Growth of European Pines. *For. Ecol. Manag.* **2015**, *343*, 101–109. [[CrossRef](#)]
18. Murphy, B.P.; Russell-Smith, J.; Prior, L.D. Frequent Fires Reduce Tree Growth in Northern Australian Savannas: Implications for Tree Demography and Carbon Sequestration. *Glob. Chang Biol.* **2010**, *16*, 331–343. [[CrossRef](#)]
19. Pausas, J.; Ouadah, N.; Ferran, A.; Gimeno, T.; Vallejo, R. Fire Severity and Seedling Establishment in *Pinus Halepensis* Woodlands, Eastern Iberian Peninsula. *Plant Ecol.* **2003**, *168*, 205–213. [[CrossRef](#)]
20. Fritts, H.C. Tree Rings and Climate. *Sci. Am.* **1972**, *226*, 92–100. [[CrossRef](#)]
21. Schweingruber, F.H. *Trees and Wood in Dendrochronology*; Springer: Berlin/Heidelberg, Germany, 1993; ISBN 9788578110796.
22. Altieri, S.; Mereu, S.; Cherubini, P.; Castaldi, S.; Sirignano, C.; Lubritto, C.; Battipaglia, G. Tree-Ring Carbon and Oxygen Isotopes Indicate Different Water Use Strategies in Three Mediterranean Shrubs at Capo Caccia (Sardinia, Italy). *Trees-Struct. Funct.* **2015**, *29*, 1593–1603. [[CrossRef](#)]
23. Martín-Benito, D.; Del Río, M.; Heinrich, I.; Helle, G.; Cañellas, I. Response of Climate-Growth Relationships and Water Use Efficiency to Thinning in a *Pinus Nigra* Afforestation. *For. Ecol. Manag.* **2010**, *259*, 967–975. [[CrossRef](#)]
24. Tareh, S.; Bai, S.H.; Abdullah, K.M.; Zalucki, J.; Nessa, A.; Omidvar, N.; Wang, D.; Zhan, J.; Wang, F.; Yang, J.; et al. Long-Term Impact of Prescribed Burning on Water Use Efficiency, Biological Nitrogen Fixation, and Tree Growth of Understory Acacia Species in a Suburban Forest Ecosystem of Subtropical Australia. *J. Soils Sediments* **2021**, *21*, 3620–3631. [[CrossRef](#)]
25. Rostami, A.; Shah-Hosseini, R.; Asgari, S.; Zarei, A.; Aghdami-Nia, M.; Homayouni, S. Active Fire Detection from Landsat-8 Imagery Using Deep Multiple Kernel Learning. *Remote Sens.* **2022**, *14*, 992. [[CrossRef](#)]
26. Avetisyan, D.; Velizarova, E.; Filchev, L. Post-Fire Forest Vegetation State Monitoring through Satellite Remote Sensing and In Situ Data. *Remote Sens.* **2022**, *14*, 6266. [[CrossRef](#)]
27. Marfella, L.; Marzaioli, R.; Paziienza, G.; Mairota, P.; Glanville, H.C.; Rutigliano, F.A. Medium-Term Effects of Wildfire Severity on Soil Physical, Chemical and Biological Properties in *Pinus halepensis* Mill. Woodland (Southern Italy): An Opportunity for Invasive Acacia Saligna Colonization? *For. Ecol. Manag.* **2023**, *542*, 121010. [[CrossRef](#)]
28. Alcaras, E.; Costantino, D.; Guastaferro, F.; Parente, C.; Pepe, M. Normalized Burn Ratio Plus (NBR+): A New Index for Sentinel-2 Imagery. *Remote Sens.* **2022**, *14*, 1727. [[CrossRef](#)]
29. Sun, Z.; Wang, L.; Chu, C.; Zhang, Y. Outlier Reconstruction of NDVI for Vegetation-Cover Dynamic Analyses. *Appl. Sci.* **2022**, *12*, 4412. [[CrossRef](#)]
30. Silvestro, R.; Saulino, L.; Cavallo, C.; Allevato, E.; Pindozi, S.; Cervelli, E.; Conti, P.; Mazzoleni, S.; Saracino, A. The Footprint of Wildfires on Mediterranean Forest Ecosystem Services in Vesuvius National Park. *Fire* **2021**, *4*, 95. [[CrossRef](#)]
31. Xiao-Rui, T.; Mcrae, D.J.; Li-Fu, S.; Ming-Yu, W.; Hong, L. Satellite Remote-Sensing Technologies Used in Forest Fire Management. *J. For. Res.* **2005**, *16*, 73–78. [[CrossRef](#)]
32. Saulino, L.; Rita, A.; Migliozi, A.; Maffei, C.; Allevato, E.; Garonna, A.P.; Saracino, A. Detecting Burn Severity across Mediterranean Forest Types by Coupling Medium-Spatial Resolution Satellite Imagery and Field Data. *Remote Sens.* **2020**, *12*, 741. [[CrossRef](#)]
33. Lutes, D.C.; Keane, R.E.; Caratti, J.F.; Key, C.H.; Benson, N.C.; Sutherland, S.; Gangi, L.J. *FIREMON: Fire Effects Monitoring and Inventory System*; USDA Forest Service, Rocky Mountain Research Station, General Technical Report; USDA Forest Service Rocky Mountain Research Station: Ogden, UT, USA, 2006; p. 164. [[CrossRef](#)]
34. Keeley, J.E. Fire Intensity, Fire Severity and Burn Severity: A Brief Review and Suggested Usage. *Int. J. Wildland Fire* **2009**, *18*, 116–126. [[CrossRef](#)]
35. Schweingruber, F.H. *Tree Rings—Basics and Applications of Dendrochronology*; Kluwer Academic: Dordrecht, The Netherlands, 1998.
36. Eckstein, D.; Bauch, J. Beitrag Zur Rationalisierung Eines Dendrochronologischen Verfahrens Und Zur Analyse Seiner Aussagesicherheit. *Forstwiss. Cent.* **1969**, *88*, 230–250. [[CrossRef](#)]
37. Biondi, F.; Qeadan, F. A Theory-Driven Approach to Tree-Ring Standardization: Defining the Biological Trend from Expected Basal Area Increment. *Tree-Ring Res.* **2008**, *64*, 81–96. [[CrossRef](#)]
38. Danise, T.; Andriuzzi, W.S.; Battipaglia, G.; Certini, G.; Guggenberger, G.; Innangi, M.; Mastrolonardo, G.; Niccoli, F.; Pelleri, F.; Fioretto, A. Mixed-Species Plantation Effects on Soil Biological and Chemical Quality and Tree Growth of a Former Agricultural Land. *Forests* **2021**, *12*, 842. [[CrossRef](#)]
39. Bunn, A.G. Statistical and Visual Crossdating in R Using the DplR Library. *Dendrochronologia* **2010**, *28*, 251–258. [[CrossRef](#)]
40. Bunn, A.G. A Dendrochronology Program Library in R (DplR). *Dendrochronologia* **2008**, *26*, 115–124. [[CrossRef](#)]
41. Muñoz-Sabater, J. *ERA5-Land Monthly Averaged Data from 1981 to Present*. Copernicus Climate Change Service (C3S) Climate Data Store; Copernicus Climate Data Store: New York, NY, USA, 2019.
42. Gorelick, N.; Hancher, M.; Dixon, M.; Ilyushchenko, S.; Thau, D.; Moore, R. Google Earth Engine: Planetary-Scale Geospatial Analysis for Everyone. *Remote Sens. Environ.* **2017**, *202*, 18–27. [[CrossRef](#)]
43. Zang, C.; Biondi, F. Treeclim: An R Package for the Numerical Calibration of Proxy-Climate Relationships. *Ecography* **2015**, *38*, 431–436. [[CrossRef](#)]

44. Meko, D.; Touchan, R.; Anchukaitis, K. Seascorr: A MATLAB Program for Identifying the Seasonal Climate Signal in an Annual Tree-Ring Time Series. *Comput. Geosci.* **2011**, *37*, 1234–1241. [[CrossRef](#)]
45. Ehleringer, J.R.; Hall, A.E.; Farquhar, G.D. *Stable Isotopes and Plant Carbon-Water Relations*; Academic Press: San Diego, CA, USA, 1993.
46. Valor, T.; Battipaglia, G.; Piqué, M.; Altieri, S.; González-Olabarria, J.R.; Casals, P. Correction to: The Effect of Prescribed Burning on the Drought Resilience of *Pinus Nigra* Ssp. *Salzmannii* Dunal (Franco) and *P. Sylvestris* L. *Ann. For. Sci.* **2020**, *77*, 22. [[CrossRef](#)]
47. R Core Team. *R: A Language and Environment for Statistical Computing*; R Foundation for Statistical Computing: Vienna, Austria, 2022.
48. Forrester, D.I.; Tachauer, I.; Annighoefer, P.; Barbeito, I.; Pretzsch, H.; Ruiz-Peinado, R.; Stark, H.; Vacchiano, G.; Zlatanov, T.; Chakraborty, T.; et al. Generalized Biomass and Leaf Area Allometric Equations for European Tree Species Incorporating Stand Structure, Tree Age and Climate. *For. Ecol. Manag.* **2017**, *396*, 160–175. [[CrossRef](#)]
49. Tabacchi, G.; Di Cosmo, L.; Gasparini, P.; Morelli, S. *Stima Del Volume e Della Fitomassa Delle Principali Specie Forestali Italiane: Equazioni Di Previsione, Tavole Del Volume e Tavole Della Fitomassa Arborea Epigea*; Consiglio per la Ricerca e la sperimentazione in Agricoltura (CRA): Rome, Italy, 2011; p. 412.
50. Picchio, R.; Tavankar, F.; Rafie, H.; Kivi, A.R.; Jourgholami, M.; Monaco, A.L. Carbon Storage in Biomass and Soil after Mountain Landscape Restoration: *Pinus Nigra* and *Picea Abies* Plantations in the Hyrcanian Region. *Land* **2022**, *11*, 422. [[CrossRef](#)]
51. IPCC. Forest Land. In *2006 IPCC Guidelines for National Greenhouse Gas Inventories Volume 4 Agriculture, Forestry and Other Land Use*; IPCC: Geneva, Switzerland, 2006; Chapter 4.
52. European Commission. *Quarterly Report on European Electricity Markets*; European Commission: Brussels, Belgium, 2022.
53. Miller, J.D.; Knapp, E.E.; Key, C.H.; Skinner, C.N.; Isbell, C.J.; Creasy, R.M.; Sherlock, J.W. Calibration and Validation of the Relative Differenced Normalized Burn Ratio (RdNBR) to Three Measures of Fire Severity in the Sierra Nevada and Klamath Mountains, California, USA. *Remote Sens. Environ.* **2009**, *113*, 645–656. [[CrossRef](#)]
54. Harvey, B.J.; Andrus, R.A.; Anderson, S.C. Incorporating Biophysical Gradients and Uncertainty into Burn Severity Maps in a Temperate Fire-Prone Forested Region. *Ecosphere* **2019**, *10*, e02600. [[CrossRef](#)]
55. Hoy, E.E.; French, N.H.F.; Turetsky, M.R.; Trigg, S.N.; Kasischke, E.S. Evaluating the Potential of Landsat TM/ETM+ Imagery for Assessing Fire Severity in Alaskan Black Spruce Forests. *Int. J. Wildland Fire* **2008**, *17*, 500–514. [[CrossRef](#)]
56. Cernusak, L.A.; Hutley, L.B.; Beringer, J.; Tapper, N.J. Stem and Leaf Gas Exchange and Their Responses to Fire in a North Australian Tropical Savanna. *Plant Cell Environ.* **2006**, *29*, 632–646. [[CrossRef](#)]
57. Schweingruber, F.H. *Wood Structure and Environment*; Springer: Berlin/Heidelberg, Germany, 2007.
58. Valor, T.; Casals, P.; Altieri, S.; González-Olabarria, J.R.; Piqué, M.; Battipaglia, G. Disentangling the Effects of Crown Scorch and Competition Release on the Physiological and Growth Response of *Pinus Halepensis* Mill. Using $\delta^{13}\text{C}$ and $\delta^{18}\text{O}$ Isotopes. *For. Ecol. Manag.* **2018**, *424*, 276–287. [[CrossRef](#)]
59. Sala, A.; Piper, F.; Hoch, G. Physiological Mechanisms of Drought-Induced Tree Mortality Are Far from Being Resolved. *New Phytol.* **2010**, *186*, 274–281. [[CrossRef](#)]
60. Nardini, A.; Casolo, V.; Borgo, A.D.; Savi, T.; Stenni, B.; Bertocin, P.; Zini, L.; McDowell, N.G. Rooting Depth, Water Relations and Non-Structural Carbohydrate Dynamics in Three Woody Angiosperms Differentially Affected by an Extreme Summer Drought. *Plant Cell Environ.* **2016**, *39*, 618–627. [[CrossRef](#)]
61. McDowell, N.; Brooks, J.R.; Fitzgerald, S.A.; Bond, B.J. Carbon Isotope Discrimination and Growth Response of old *Pinus Ponderosa* Trees to Stand Density Reductions. *Plant Cell Environ.* **2003**, *26*, 631–644. [[CrossRef](#)]
62. van Mantgem, P.J.; Falk, D.A.; Williams, E.C.; Das, A.J.; Stephenson, N.L. Pre-Fire Drought and Competition Mediate Post-Fire Conifer Mortality in Western U.S. National Parks. *Ecol. Appl.* **2018**, *28*, 1730–1739. [[CrossRef](#)]
63. van Mantgem, P.J.; Nesmith, J.C.B.; Keifer, M.; Knapp, E.E.; Flint, A.; Flint, L. Climatic Stress Increases Forest Fire Severity Across the Western United States. *Ecol. Lett.* **2013**, *16*, 1151–1156. [[CrossRef](#)] [[PubMed](#)]
64. McDowell, N.G. Mechanisms Linking Drought, Hydraulics, Carbon Metabolism, and Vegetation Mortality. *Plant Physiol.* **2011**, *155*, 1051–1059. [[CrossRef](#)] [[PubMed](#)]
65. Khan, M.N.; Gong, Y.; Hu, T.; Lal, R.; Zheng, J.; Justine, M.F.; Azhar, M.; Che, M.; Zhang, H. Effect of Slope, Rainfall Intensity and Mulch on Erosion and Infiltration under Simulated Rain on Purple Soil of South-Western Sichuan Province, China. *Water* **2016**, *8*, 528. [[CrossRef](#)]
66. Zeppel, M.J.B.; Wilks, J.V.; Lewis, J.D. Impacts of Extreme Precipitation and Seasonal Changes in Precipitation on Plants. *Biogeosciences* **2014**, *11*, 3083–3093. [[CrossRef](#)]
67. Farquhar, G.D.; O’Leary, M.H.; Berry, J.A. On the Relationship Between Carbon Isotope Discrimination and the Inter-cellular Carbon Dioxide Concentration in Leaves. *Aust. J. Plant Physiol.* **1982**, *9*, 121–137. [[CrossRef](#)]
68. McDowell, N.; Pockman, W.T.; Allen, C.D.; Breshears, D.D.; Cobb, N.; Kolb, T.; Plaut, J.; Sperry, J.; West, A.; Williams, D.G.; et al. Mechanisms of Plant Survival and Mortality During Drought: Why Do Some Plants Survive While Others Succumb to Drought? *New Phytol.* **2008**, *178*, 719–739. [[CrossRef](#)]
69. Tardieu, F.; Simonneau, T. Variability among Species of Stomatal Control under Fluctuating Soil Water Status and Evaporative Demand: Modelling Isohydic and Anisohydic Behaviours. *J. Exp. Bot.* **1998**, *49*, 419–432. [[CrossRef](#)]
70. Fernandes, P.M.; Vega, J.A.; Jiménez, E.; Rigolot, E. Fire Resistance of European Pines. *For. Ecol. Manag.* **2008**, *256*, 246–255. [[CrossRef](#)]

71. Jia, H.; Guan, C.; Zhang, J.; He, C.; Yin, C.; Meng, P. Drought Effects on Tree Growth, Water Use Efficiency, Vulnerability and Canopy Health of *Quercus Variabilis*-*Robinia Pseudoacacia* Mixed Plantation. *Front. Plant Sci.* **2022**, *13*, 1018405. [[CrossRef](#)]
72. Driesen, E.; Van den Ende, W.; De Proft, M.; Saeyns, W. Influence of Environmental Factors Light, CO₂, Temperature, and Relative Humidity on Stomatal Opening and Development: A Review. *Agronomy* **2020**, *10*, 1975. [[CrossRef](#)]
73. Richardson, F.; Brodribb, T.J.; Jordan, G.J. Amphistomatic Leaf Surfaces Independently Regulate Gas Exchange in Response to Variations in Evaporative Demand. *Tree Physiol.* **2017**, *37*, 869–878. [[CrossRef](#)] [[PubMed](#)]
74. Salmon, Y.; Torres-Ruiz, J.M.; Poyatos, R.; Martínez-Vilalta, J.; Meir, P.; Cochard, H.; Mencuccini, M. Balancing the Risks of Hydraulic Failure and Carbon Starvation: A Twig Scale Analysis in Declining Scots Pine. *Plant Cell Environ.* **2015**, *38*, 2575–2588. [[CrossRef](#)] [[PubMed](#)]
75. Deslauriers, A.; Caron, L.; Rossi, S. Carbon Allocation during Defoliation: Testing a Defense-Growth Trade-off in Balsam Fir. *Front. Plant Sci.* **2015**, *6*, 338. [[CrossRef](#)] [[PubMed](#)]
76. Bouzidi, H.A.; Balducci, L.; Mackay, J.; Deslauriers, A. Interactive Effects of Defoliation and Water Deficit on Growth, Water Status, and Mortality of Black Spruce (*Picea Mariana* (Mill.) B.S.P.). *Ann. For. Sci.* **2019**, *76*, 21. [[CrossRef](#)]
77. Vanderklein, D.W.; Reich, P.B. The Effect of Defoliation Intensity and History on Photosynthesis, Growth and Carbon Reserves of Two Conifers with Contrasting Leaf Lifespans and Growth Habits. *New Phytol.* **1999**, *144*, 121–132. [[CrossRef](#)]
78. Krause, C.; Morin, H. Changes in Radial Increment in Stems and Roots of Balsam Fir [*Abies Balsamea* (L.) Mill.] after Defoliation Spruce Budworm. *For. Chron.* **1995**, *71*, 747–754. [[CrossRef](#)]
79. Souza, C.R.; Maia, V.A.; Mariano, R.F.; de Souza, F.C.; Araújo, F.d.C.; de Paula, G.G.; Menino, G.C.d.O.; Coelho, P.A.; Santos, P.F.; Morel, J.D.; et al. Tropical Forests in Ecotonal Regions as a Carbon Source Linked to Anthropogenic Fires: A 15-Year Study Case in Atlantic Forest—Cerrado Transition Zone. *For. Ecol. Manag.* **2022**, *519*, 120326. [[CrossRef](#)]
80. Kala, C.P. Environmental and Socioeconomic Impacts of Forest Fires: A Call for Multilateral Cooperation and Management Interventions. *Nat. Hazards Res.* **2023**, *3*, 286–294. [[CrossRef](#)]
81. Intergovernmental Panel on Climate Change, IPCC. *Global Warming of 1.5 °C*; An IPCC Special Report; IPCC: Geneva, Switzerland, 2018.
82. Taye, F.A.; Folkersen, M.V.; Fleming, C.M.; Buckwell, A.; Mackey, B.; Diwakar, K.; Le, D.; Hasan, S.; Ange, C.S. The Economic Values of Global Forest Ecosystem Services: A Meta-Analysis. *Ecol. Econ.* **2021**, *189*, 107145. [[CrossRef](#)]
83. Roces-Díaz, J.V.; Santín, C.; Martínez-Vilalta, J.; Doerr, S.H. A Global Synthesis of Fire Effects on Ecosystem Services of Forests and Woodlands. *Front. Ecol. Environ.* **2022**, *20*, 170–178. [[CrossRef](#)]

Disclaimer/Publisher’s Note: The statements, opinions and data contained in all publications are solely those of the individual author(s) and contributor(s) and not of MDPI and/or the editor(s). MDPI and/or the editor(s) disclaim responsibility for any injury to people or property resulting from any ideas, methods, instructions or products referred to in the content.